Available online at www.sciencedirect.com

Manufacturing Letters

Manufacturing Letters 41 (2024) 546–557

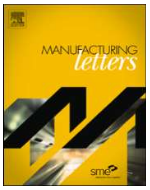

52nd SME North American Manufacturing Research Conference (NAMRC 52, 2024)

Investigation of Experimental Parameters in the Electric Field and Mechanical Vibration Integrated AFM-Based Nanopatterning on PEDOT

Mohammad Alshoul, Xinchen Wang, Zimo Wang, Jia Deng*

Department of Systems Science and Industrial Engineering, Thomas J. Watson College of Engineering and Applied Science, Binghamton University, Binghamton, NY 13902, USA

* Corresponding author. *E-mail address:* jiadeng@binghamton.edu.

Abstract

Atomic force microscope (AFM)-based nanomanufacturing offers an affordable and easily deployable method for fabricating high-resolution nanopatterns. This study employs a comprehensive design of experiment (DOE) approach to investigate the effects of various parameters, such as voltage, speed, and vibration axis, on the width and depth of lithography patterns using electrical field and vibration-assisted lithography on PEDOT: PSS films. The DOE explores the effect of voltage and speed on the process of electrical field and vibration-assisted AFM-based nanopatterning in two vibration trajectories: a circular trajectory employing X and Y axis vibration and a reciprocating trajectory employing Y axis vibration. The results indicate that using circular XY-vibration with a low stiffness contact probe and optimized speed and voltage factors results in higher depth and width of the lithography patterns compared to Y-vibration alone at the same parameters as expected. In both cases, pattern width was dominantly controlled by the voltage. Regarding depth, in XY-vibration, the speed of the tip is the most significant factor, while for Y-vibration, voltage plays the most significant role. It is noteworthy that there is a minimum threshold of speed that can produce a pattern; for example, the high-speed level that produced patterns in the circular trajectory (XY-vibration) did not produce patterns in reciprocating motion (Y-vibration). In conclusion, the study demonstrates the significant impact of voltage, speed, and axis on the width and depth of the lithography patterns. These findings can be instrumental in developing and understanding AFM-based high-resolution nanofabrication techniques.

Keywords: Atomic force microscope; Nanomanufacturing; Nanopatterning; Lithography; Electric field; Vibration

1. Introduction

Nanotechnologies have significantly advanced various research fields, including fundamental science, microelectronics, optics, and plastics, providing diverse applications [1]. Achieving consistent and swift fabrication of high-resolution nanofeatures is critical for the development of nanoelectronics, such as microelectromechanical systems and nanoelectromechanical systems (MEMS and NEMS), photonic and bio-nanotechnological devices [2]. One of the promising and rapidly emerging fields is organic electronics. It has drawn much interest as a technological platform by using the special qualities of organic materials to make mechanically flexible, lightweight, and affordable devices. Organic thin-film transistors (OTFTs) [3,4], organic solar cells [5,6], organic light-emitting diodes (OLEDs) [7], and sensors [3-9] are examples of such devices, where material such as PEDOT: PSS could be considered as an organic semiconductor, combines cationic poly (3,4-ethylene dioxythiophene) with poly(4-styrene sulfonate) anion which offer excellent conductivity, oxidation resistance, and transparency, making it an ideal candidate for electromagnetic shielding, noise suppression, and optical applications [10]. Nanolithography encompasses the creation of nanoscale patterns on materials or substrates through various nanofabrication or nanopatterning techniques. This field is dedicated to fabricating and utilizing these patterns for various applications [11]. Masked lithography enables efficient pattern fabrication on substrate materials, but these methods require masks fabricated using maskless lithography approaches. [12]. There are a variety of maskless surface patterning and nanolithography techniques [13], such as nanoimprint lithography (NIL) [14], scanning probe lithography (SPL) [15], atomic force microscope (AFM) nanolithography [16], extreme ultraviolet lithography (EUVL) [17], and X-ray Lithography [18].

In AFM-based nanopatterning techniques, vibration-assisted nanomachining is a prominent nanopatterning technique [19,20]. The utilization of vibrations facilitates the creation of complex 2D and 3D intricate patterns [21,22], eases the patterning process, and reduces tip wear. This technique also provides the flexibility of adjustable nanomachining procedures [23-26]. SEM analysis revealed a pronounced reduction of tip wear in ultrasonic vibration-assisted nanomachining relative to its non-vibrational counterpart, as evidenced by diminished post-machining tip radius enlargement. This underscores the efficacy of ultrasonic vibrations in the reduction of frictional forces during nanomachining, thereby prolonging tool longevity and enhancing operational efficacy additionally. It plays a pivotal role in enhancing the overall performance of nanomachining processes, resulting in accelerated patterning. This is explained by [27] as the periodic separation between the tool rake face and uncut material in vibration-assisted machining, which leads to reduced machining forces and chip thickness; furthermore, it helps mitigate thermo-chemical wear mechanisms. This multifaceted approach to nanopatterning broadens the scope of achievable geometries and optimizes the efficiency of nanomachining procedures. A study [28] confirmed the effectiveness of vibration-assisted nanomachining in generating 3D master nano-templates for soft lithography. Another innovative approach [29] utilized vibration-assisted sample heating with a standard AFM probe for thermal AFM nanolithography, which eliminates the requirement for specialized thermal probes. AFM can be used as a direct scratching tool on conductive polymers, which achieved high-resolution patterns of PEDOT: PSS on both rigid and flexible substrates [30].

Moreover, integrating an electric field with AFM enables the rapid creation of features on polymer films. This method involves localized softening of tiny polymer volumes through Joule heating and manipulation using non-uniform electric field gradients, allowing for quick feature generation. The single-step process with conventional AFM equipment eliminates the need for external heating or AFM tip-film contact [31,32]. The AFM probe and the sample surface are kept as the electrochemical anodic reaction's cathode and anode during the electric field-induced process. Water molecules bind to sample surfaces to act as the electrolyte in oxidation reactions whenever hydroxyl ions are required [33], which creates a liquid meniscus bridge between the probe and the intended surface [34]. Our previous study [35], a contact mode electric field-assisted AFM lithography method, employs a soft probe to make patterns on polymer substrates. By applying a setpoint force of 0.5-1 nN to the AFM tip, nanoholes and nanopatterns with adjustable feature dimensions were achieved. In another study [36], we provided a comparison of adjustable vibration parameters for the lithography of PMMA film in terms of the axis of the vibration relative to the feed speed and the vibration amplitude of the piezo actuator used.

This study focuses on nanomachining parameters of electrical field and mechanical vibration-assisted AFM-based nanopatterning process on a conductive polymer PEDOT: PSS, utilizing design of experiment (DOE) analysis and analysis of variance (ANOVA) to identify factors affecting lithography pattern dimensions. ANOVA is chosen for its ability to analyze multiple factors simultaneously, making it suitable for DOE approaches in experimental design studies.

Nomenclature

AFM	atomic force microscopy
E-AFM	electrical atomic force microscopy
DOE	design of experiment
ANOVA	analysis of variance
C-AFM	conductive atomic force microscopy

2. Experimental setup and process model

The experimental configuration comprised a Park Systems AFM (XE7, Park Systems Corporation, Suwon, South Korea) for nanoscale scanning and lithography. The AFM was enclosed in an acoustic chamber with an ambient temperature of 24°C and a 15% relative humidity. Specifically, we investigated the application of a low-stiffness conductive contact probe (tip) CSG10-pt, with a nominal radius of 35 nm, featuring a spring constant of 0.11 N/m connected to a voltage power supply to establish the electric field potential within the setup configuration required for the tip bias lithography. Additionally, a custom-manufactured nanolithography stage was utilized, featuring two piezoelectric actuators positioned along the X and Y axes. These actuators were affixed between the extruded piler and side sections of the aluminum stage, as illustrated in Fig. 1. To drive the piezoelectric actuators and cause vibration in the designated axis, a signal generator (USB-6259, National Instruments, Austin, TX, USA) and two signal amplifiers (PX200, PiezoDrive, Shortland, NSW, Australia) with a gain of 20 each were employed.

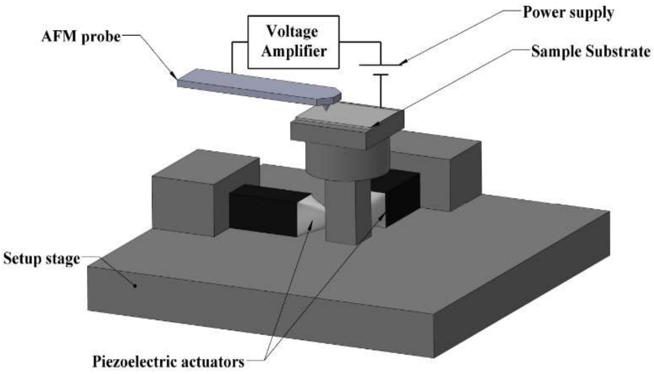

Fig. 1. Schematic diagram of the experimental setup for electrical field and vibration-assisted AFM-based nanopatterning.

The XY-piezoelectric actuators are subjected to sinusoidal signals produced by National Instruments (USB-6259). Employing uniform driving signal amplitudes and a 90-degree phase differential, the pillar undergoes circular trajectory vibrations. This setup offers control over the amplitude of the vibration, the axis of the vibration, and the frequency of that amplitude, as illustrated in Fig. 2.

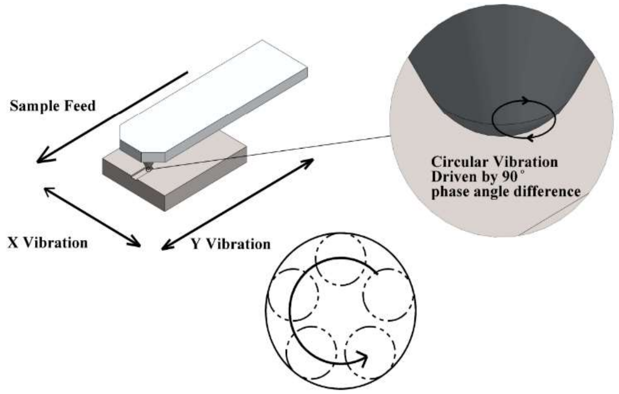

Fig. 2. The circular trajectory introduced by XY-vibration.

The experiment utilized fixed vibration parameters for the piezoelectric actuators of 2 kHz frequency and 0.2 Vpp amplitude for both the X and Y axes. A PEDOT: PSS film, spin-coated on a highly doped silicon substrate, was prepared from a PEDOT: PSS aqueous solution (Clevios PH 1000) with a 1:2.5 ratio, forming a 65 nm thick film with a typical conductivity of 850 S/cm. The process model, shown in Fig. 3, incorporates electric field and vibration assistance. Investigated inputs (Xs) include probe speed (the speed parallel to the sample feed shown in Fig. 2) and the voltage for the electrical field. Tunable factors like vibration’s amplitude and frequency, setpoint, temperature, and humidity were held constant. Non-tunable factors, like surface roughness, system stability, and the tip used, may introduce variability in the output of the lithography. Outputs (Ys) include trench width and depth on PEDOT films. Experiments were conducted with two vibration choices: XY-vibration and Y-vibration—both were evaluated in the DOE study, as indicated by the dotted line in Fig. 3.

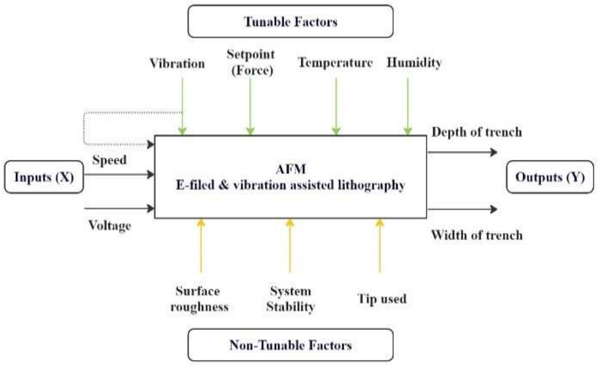

Fig. 3. Electrical field and vibration-assisted AFM-based nanopatterning process model.

3. Design of experiments

Multiple DOE studies were conducted to investigate a wide range of parameters and their effects. For these studies, the applied normal force was fixed to be 2 nN. The first DOE included 2 levels of sample feed speed factor by 3 levels of voltage factor, the vibration drive was circular as mentioned with XY-vibration in the amplitude of 0.2 Vpp and 2 kHz. Each set had 3 replications as shown in Table. 1.

Table 1. DOE number 1 with 2 levels of sample speeds 3 levels of voltages and XY-vibration.

Factor	Levels
Speed	0.25 μm/s
	1.25 μm/s
Voltage	0.5 V
	1.0 V
	1.5 V

Secondly, the second DOE introduced 3 levels of speed and 3 levels of voltage, while the vibration drive was only in the Y axis with an amplitude of 0.2 Vpp at the frequency of 2000 Hz, as presented in Table 2. The intermediate speed level was introduced because the high-level speed (1.25 μm/s) did not produce patterns at lower voltages and resulted in zero values data sets due to the exclusion of the X-vibration. Each pair of the parameters had 3 replicates, resulting in 18 runs in the first DOE design and 27 runs for the second DOE design. The DOE analysis will consider the voltage and speed as the dominant controlling factors in the first and second DOEs. Then, a combination of the two DOE studies will be introduced with the controlling factor of the number of axes for the vibration to investigate the differences between the XY-vibration and Y-vibration alone. This is due to understanding the potential of minimizing the width of the trenches by excluding the X-vibration; however, another tuning with parameters will be required to compensate for the exclusion of X-vibration as it is not able to create patterns at lower voltages and high speeds.

Table 2. DOE number 1 with 2 levels of speeds and 3 levels of voltages and Y-vibration.

Factor	Levels
Speed	0.25 μm/s
	0.5 μm/s
	1.25 μm/s
Voltage	0.5 V
	1.0 V
	1.5 V

For the DOE study, we incorporate the previous DOE data sets and consider the vibration as a factor, as presented in Table 3. Note that the intermediate speed was introduced in the Y-vibration only.

Table 3. Nested DOE includes the axis factors in addition to the speed and voltage.

Factor	Levels
Speed	0.25 μm/s
	0.5 μm/s*
	1.25 μm/s
Voltage	0.5 V
	1.0 V
	1.5 V
Axis	1 axis (Y)
	2 axis (XY)

**Indicates intermediate level introduced in Y vibration only*

A sample of the PEDOT: PSS film topology is presented in Fig. 4. The surface topology and the average profile of the film surface show variability in height (roughness), and it measured (0.439 nm) average root mean square roughness across a sample before lithography. This roughness is anticipated at this level of thickness.

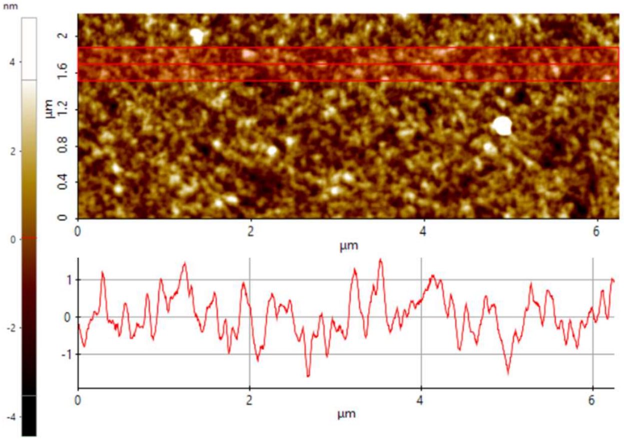

Fig. 4. The topology of PEDOT: PSS film and the average height profile.

4. Results and discussion

4.1 The analysis of the XY-vibration DOE

The initial design of the DOE involves presenting data sets representing X-vibration and Y-vibration used in the circular trajectory drive. These sets were measured from lithography patterns and are detailed in Table 4. We have tested the normality of the surface geometry measurements (widths and depths) via the Ryan-Joiner normality tests.

Table 4. First DOE data set for XY-vibration.

Pattern	Voltage (V)	Speed (μm/s)	Avg Depth (nm)	Avg width (nm)
1	0.5	0.25	4.1	99.3
2	0.5	1.25	5	119.3
3	1	0.25	7.2	145.0
4	1	1.25	5.7	116.7
5	1.5	0.25	8	152.0
6	1.5	1.25	5	127.7
7	0.5	0.25	4.2	114.3
8	0.5	1.25	3.6	98.3
9	1	0.25	5.7	150.7
10	1	1.25	4.2	151.0
11	1.5	0.25	6.3	172.7
12	1.5	1.25	4.3	133.0
13	0.5	0.25	5.2	90.7
14	0.5	1.25	5.6	130.3
15	1	0.25	5.8	108.0
16	1	1.25	4.3	95.0
17	1.5	0.25	6.9	154.7
18	1.5	1.25	5	142.0

Additionally, the topology of the patterns is depicted in Fig. 5. In total, 18 runs have been conducted, revealing resolutions with depths ranging from 3.5 nm to 8 nm and widths varying from 90 nm to 172 nm.

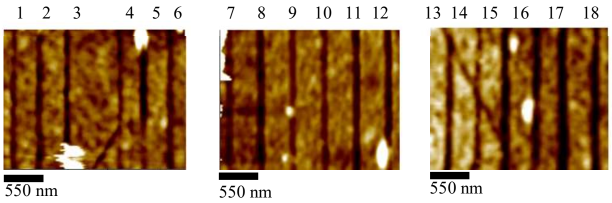

Fig. 5. The topology of XY-vibration DOE patterns.

A Pareto chart illustrating the standardized effect for each parameter with α level of 0.05 is presented in Fig. 6.

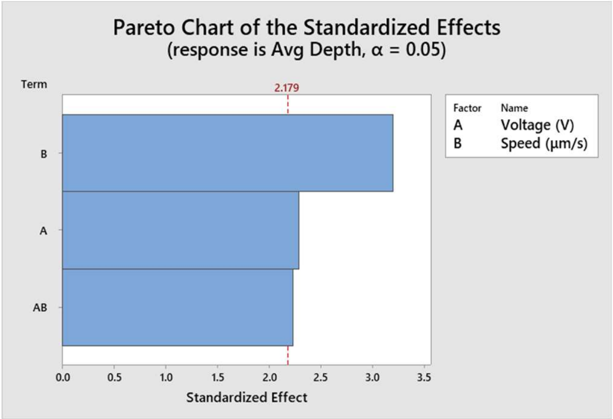

Fig. 6. Pareto chart of the standardized effect for the depth in the XY-vibration DOE.

It implied that the speed had the highest standardized effect on depth, followed by the voltage and then the interaction of the voltage and speed. The results show that all the voltage, speed, and interaction are statistically significant at the given α level of 0.05. The ANOVA results show that p-values are lower than 0.05 for the voltage, the speed, and the interaction, as shown in Table 5. These results could be explained by the time dependency of the electrical field.

Table 5. Depth ANOVA table for the first DOE with the XY vibration.

Source	DF	Adj SS	Adj MS	F-Value	P-Value
Model	5	16.649	3.3299	5.35	0.008
Linear	3	11.618	3.8728	6.22	0.009
Voltage (V)	2	5.258	2.6289	4.22	**0.041**
Speed (μm/s)	1	6.361	6.3606	10.21	**0.008**
2-Way Interactions	2	5.031	2.5156	4.04	**0.046**
Voltage (V)*Speed (μm/s)	2	5.031	2.5156	4.04	0.046
Error	12	7.473	0.6228		
Total	17	24.123			

The main effect plot in Fig. 7a illustrates the relationship between the input parameters and the output parameters for the depth, specifically a positive correlation for voltage and a negative correlation with speed. Similarly, in Fig. 7b, the interaction plot shows the effect of the interaction between the speed and voltage, and there is an interaction between the first two levels of voltages (0.5 V and 1.0 V) at 0.25 μm/s speed. The voltage shows slight to no variations across the high speed (1.25 μm/s).

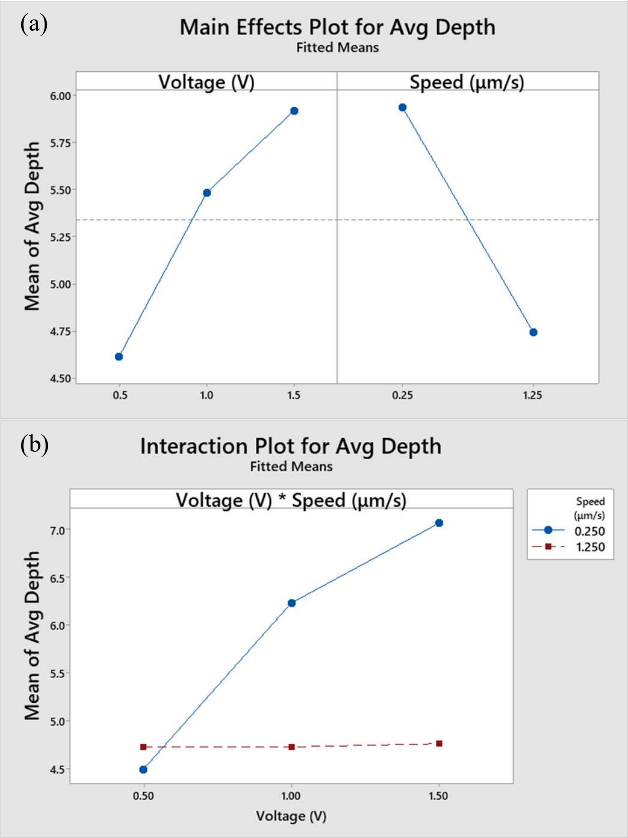

Fig. 7. (a) Main effect plot of average depth in XY-vibration DOE. (b) Interaction plot of average depth in XY-vibration DOE.

As for the width, the Pareto chart in Fig. 8 presents the standardized effect for each parameter at a significance level α of 0.05. It concludes that voltage exhibits the only highest standardized significant effect on width while the other effects weren't significant at the α level of 0.05.

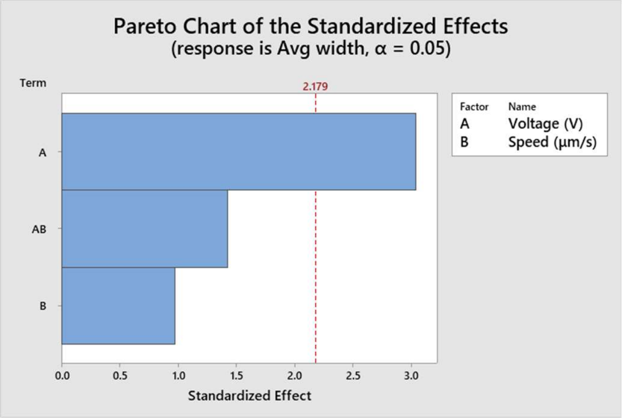

Fig. 8. Pareto chart of the standardized effect for the width in XY-vibration DOE.

Parallelly, the voltage had the only p-value less than 0.05 in the ANOVA table, as shown in Table 6.

ANOVA is employed in the study to identify significant factors affecting lithography pattern dimensions, assess interactions among parameters, and optimize experimental conditions. By quantifying variability and conducting statistical tests, ANOVA aids in understanding and improving the AFM-based nanopatterning process. Its use enables data-driven decisions for enhancing pattern quality and process efficiency.

Table 6. Width ANOVA table for the first DOE with the XY-vibration.

Source	DF	Adj SS	Adj MS	F-Value	P-Value
Model	5	5974.1	1194.8	3.73	0.029
Linear	3	4700.8	1566.9	4.89	0.019
Voltage (V)	2	4396.5	2198.3	6.87	**0.010**
Speed (μm/s)	1	304.3	304.3	0.95	0.349
2-Way Interactions	2	1273.3	636.6	1.99	0.180
Voltage (V)*Speed (μm/s)	2	1273.3	636.6	1.99	0.180
Error	12	3841.6	320.1		
Total	17	9815.8			

Regarding the relationship between voltage, speed, and width, the main effect plot in Fig. 9a emphasizes the main effect plot of voltage and speed with width. Specifically, a positive correlation is evident for voltage, and a negative correlation is observed for speed; similarly to the depth, an interaction is noted in the first two voltage levels (0.5 V and 1.0 V) at a speed of 0.25 μm/s. However, it is noteworthy that voltage exhibits significant variation in width at high speeds (1.25 μm/s) compared to the depth. This could be explained by the nature of the material removal process using the electrical bias. The experimental results imply that the voltage has a dominant effect on depth at low speeds due to the full establishment of the bias between the tip and the substrate.

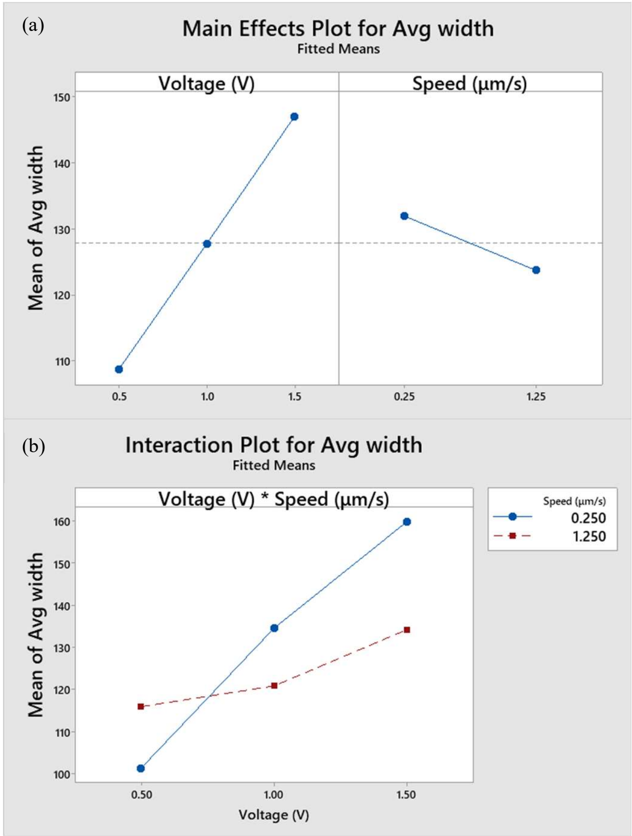

Fig. 9. (a) Main effect plot of average width in XY-vibration DOE. (b) Interaction plot of average width in XY-vibration DOE.

4.2 The analysis of Y-vibration DOE

In the second DOE, data sets utilize only the Y axis to drive a reciprocating trajectory. A total of 27 runs have been conducted, revealing resolutions with depths ranging from 3.3 nm to 5.3 nm and widths varying from 55 nm to 160 nm. Remarkably, these values are lower than those obtained with the XY-vibration circular trajectory, as presented in the data sets in Table 7.

Table 7. Second DOE data set for Y-vibration only.

Pattern	Voltage (V)	Speed (μm/s)	Avg Depth (nm)	Avg width (nm)
1	0.5	0.25	3.9	61.7
2	0.5	0.25	4.0	62.3
3	0.5	0.25	3.8	60.0
4	1	0.25	4.6	82.3
5	1	0.25	4.4	97.7
6	1	0.25	4.2	91.0
7	1.5	0.25	4.8	123.0
8	1.5	0.25	4.4	149.0
9	1.5	0.25	4.8	159.7
10	0.5	0.5	3.8	67.3
11	0.5	0.5	3.3	55.7
12	0.5	0.5	*	*
13	1	0.5	3.8	99.0
14	1	0.5	3.9	82.0
15	1	0.5	3.8	87.0
16	1.5	0.5	4.9	120.0
17	1.5	0.5	5.0	124.3
18	1.5	0.5	5.3	118.7
19	0.5	1.25	*	*
20	0.5	1.25	*	*
21	0.5	1.25	*	*
22	1	1.25	*	*
23	1	1.25	*	*
24	1	1.25	3.8	61.0
25	1.5	1.25	5.2	88.7
26	1.5	1.25	4.8	72.0
27	1.5	1.25	4.1	81.7

These datasets were acquired from lithography patterns. Topology is portrayed in Fig. 10 where a) is the 0.25 μm/s Speed patterns, b) is the 0.5 μm/s speed, and c) is 1.25 μm/s.

Analogous to the first DOE, a Pareto chart is presented in Fig. 11. illustrating the standardized effect for each parameter at an α level of 0.05. The implication is that voltage had the highest significant standardized effect on depth while the speed and the interaction between speed and voltage effect weren't significant.

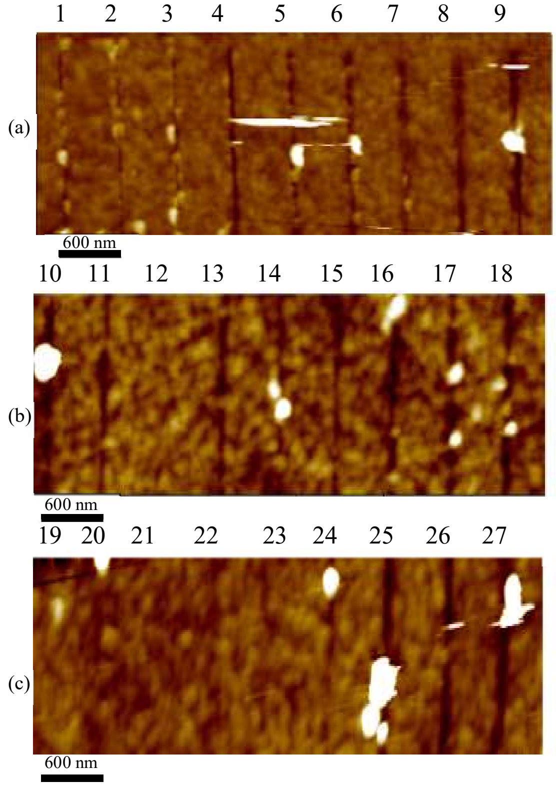

Fig. 10. The topology of the patterns with lithography speed of (a) 0.25 μm/s, (b) 0.5 μm/s, and (c) 1.25 μm/s.

However, it should be noted that a high level of speed in Y-vibration must be controlled more delicately since a higher voltage would need to be applied, as results show in Fig. 10c. High speed didn't produce patterns at low and medium voltages.

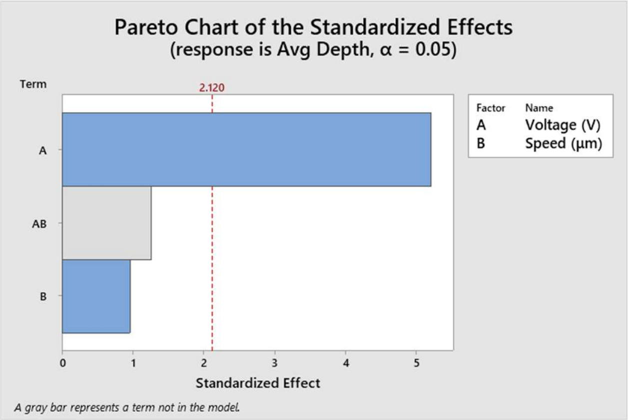

Fig. 11. Pareto chart of the standardized effect for the depth in Y-vibration DOE.

The ANOVA results for the new dataset for Y-vibration only vibration indicate p-values < 0.05 for voltage only, while the p-values for speed and the interaction were greater than 0.05, as detailed in Table 8 and Fig. 11.

Table 8. Second DOE data set for Y-vibration only.

Source	DF	Adj SS	Adj MS	F-Value	P-Value
Model	4	4.4163	1.10409	9.22	0.000
Linear	4	4.4163	1.10409	9.22	0.000
Voltage (V)	2	4.2599	2.12993	17.78	**0.000**
Speed (µm/s)	2	0.2687	0.13435	1.12	0.350
Error	16	1.9169	0.11980		
Lack-of-Fit	3	0.8012	0.26706	3.11	0.063
Pure Error	13	1.1157	0.08582		
Total	20	6.3332			

The main effect plot presented in Fig. 12a highlights a positive correlation with voltage and a negative correlation with speed versus depth. Fig. 12b depicts the interaction plot, showcasing the influence of the interaction between speed and voltage. Notably, there is a discernible interaction between the last two voltage levels (1.0 V and 1.5 V) at a speed of 0.25 µm/s and 0.5 µm/s.

We observed missing data in the dataset, attributed to the inability of material removal at low and high voltage levels, particularly evident in lines 12, 19, 20, 21, 22, and 23 as shown in Fig. 10. This highlights a limitation of single axis vibration at high speed. Notably, a circular trajectory facilitates the distribution of the electrical field along the tip trajectory, which could enhance the process of high-speed machining.

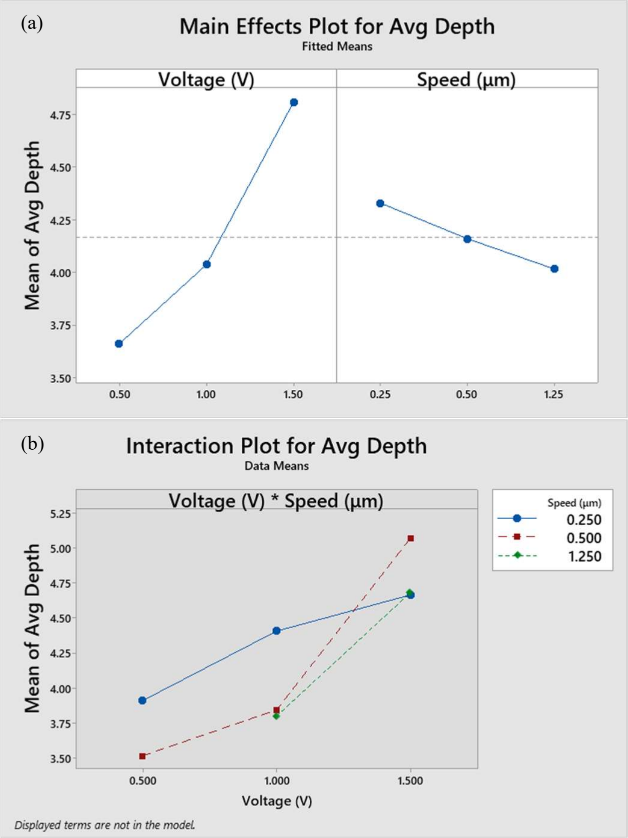

Fig. 12. (a) Main effect plot of average depth in Y vibration DOE. (b) Interaction plot of average depth in Y vibration DOE.

For the width and based on the data from Y-vibration, the Pareto chart in Fig. 13 illustrates the standardized effect for each parameter at a significance level (α) of 0.05.

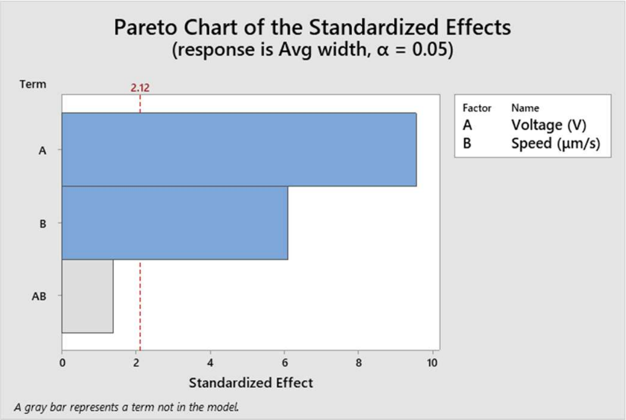

Fig. 13. Pareto chart of the standardized effect for the width in Y-vibration DOE.

It can be inferred that voltage exhibits the highest standardized and significant effect on width, followed by speed, having a standardized significant effect. It is evident that, unlike XY-vibration, where the speed significantly affected the width, Y-vibration results can only be explained by the nature of the reciprocating motion of the tip rather than a circular motion.

The main effect plot illustrated in Fig. 14a reveals the emphasis on a positive correlation with voltage and a negative correlation with speed concerning width.

Similarly, in Fig. 14b, the interaction plot displays the impact of the interaction between speed and voltage. It is evident that at the first two levels of voltages, the width didn't change significantly at 0.25 μm/s and 0.5 μm/s, while at the highest voltage level, the width increased notably at the low speed of 0.25 μm/s.

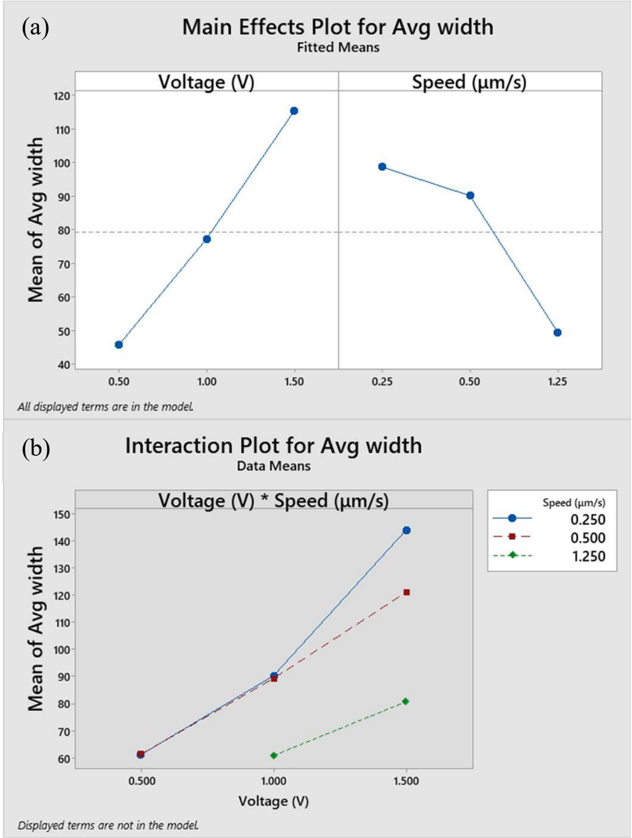

Fig. 14. (a) Main effect plot of average width in Y-vibration DOE. (b) Interaction plot of average depth in Y-vibration DOE.

4.3 Combination of the two datasets and introducing the axis of vibration as an input factor

The final DOE is conducted based on the previously presented datasets. However, the analysis features the vibration axis as a factor, as the X-vibrations in the lithography process are expected to increase the width due to the introduction of a circular trajectory motion. However, these circular trajectory motion enables patterning the materials at lower voltages and higher speeds, as evident in the second DOE study where similar low levels of voltages and high speeds didn't produce any patterns when only the Yvibration was driving the sample reciprocating. However, high-resolution patterns can be obtained when only Y-vibration is used.

The data analysis for the combined dataset, the Pareto chart in Fig. 15, presents the standardized effect for each parameter at a significance level (α) of 0.05.

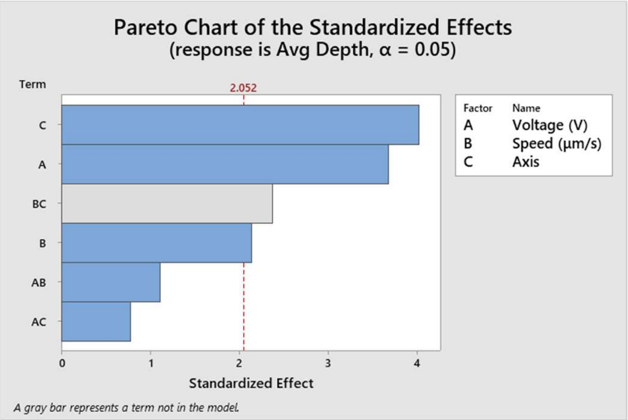

Fig. 15. Pareto chart of the standardized effect for the depth in combined DOE datasets.

It is inferred that the driving axis exhibits the highest standardized effect on depth followed by the voltage, the speed-axis interaction, and speed, and similarly, in the ANOVA table, the p-value for the factors is < 0.05, provided in Table 9.

Table 9. Depth ANOVA table for Combined DOE study.

Source	DF	Seq SS	Contribution	Adj SS	Adj MS	F-Value	P-Value
Model	11	27.63	68%	27.63	2.51	5.21	0.00
Linear	5	24.63	61%	19.30	3.86	8.01	0.00
Voltage (V)	2	6.76	17%	8.67	4.34	9.00	**0.00**
Speed (μm/s)	2	6.03	15%	3.47	1.74	3.60	**0.04**
Axis	1	11.84	29%	7.81	7.81	16.21	**0.00**
2-Way Interactions	6	3.00	7%	3.00	0.50	1.04	0.42
Voltage (V)*Speed (μm/s)	4	2.19	5%	2.62	0.66	1.36	0.27
Voltage (V)*Axis	2	0.81	2%	0.81	0.40	0.84	0.44
Error	27	13.01	32%	13.01	0.48		
Lack-of-Fit	2	4.42	11%	4.42	2.21	6.44	0.01
Pure Error	25	8.59	21%	8.59	0.34		
Total	38	40.64	100%				

The main effect plot for the combined dataset is illustrated in Fig. 16.a, And it shows a positive correlation for the voltage, a negative correlation for speed, and a positive correlation for the axis. Notably, a single axis here implies Y-vibration only, and the results would vary significantly if only the X-vibration were used where a zig-zag trajectory would be achieved that way which contributes more to more width.

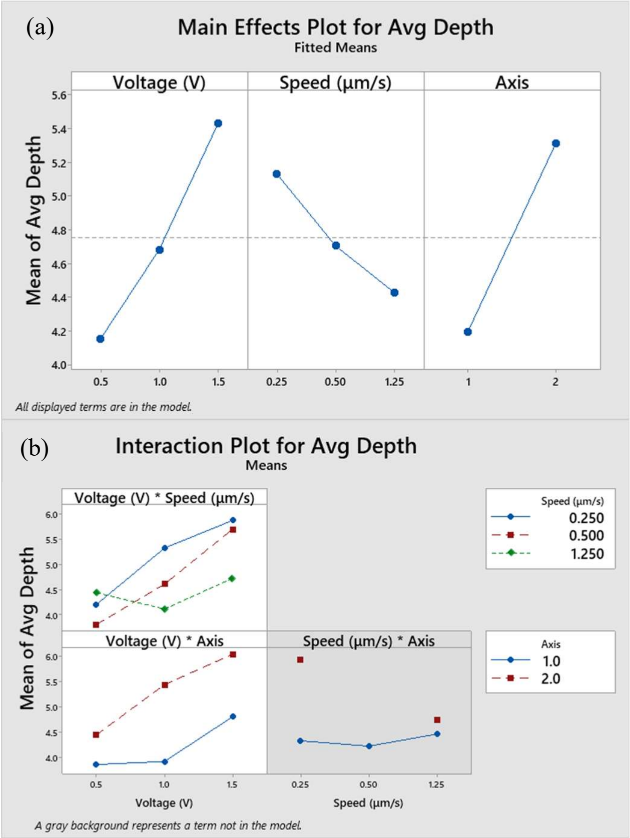

Fig. 16. (a) Main effect plot of average depth in combined DOE dataset. (b) Interaction plot of average depth in combined DOE dataset.

The interaction plot implies an interaction in the first two levels of voltage at high speed. We notice that the depths have a high average across both the voltages and speed, similarly for the width Fig. 17. The highest standardized effect was for the axis, followed by voltage and voltage-speed interaction, emphasizing the effect of trajectory on the width of the pattern. Similarly, the Width ANOVA is presented in Table 10 to showcase the model and p-values of the significant factors.

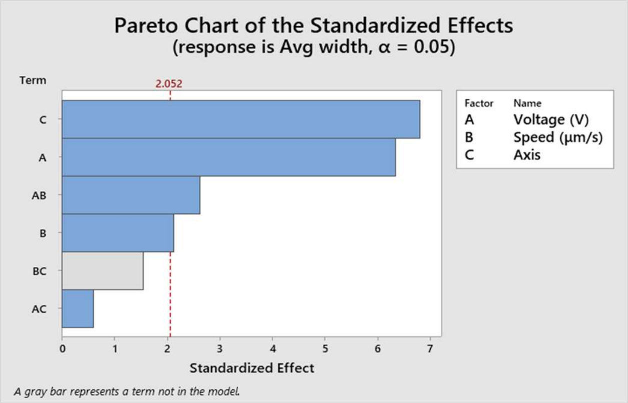

Fig. 17. Pareto chart of the standardized effect for the width in combined DOE datasets.

Table 10. Width ANOVA table for Combined DOE study.

Source	DF	Seq SS	Contribution	Adj SS	Adj MS	F-Value	P-Value
Model	11	33476.4	84.30%	33476.4	3043.3	13.18	0.000
Linear	5	29100.4	73.28%	22585.3	4517.1	19.57	0.000
Voltage (V)	2	10796.2	27.19%	11278.9	5639.4	24.43	**0.000**
Speed (µm/s)	2	3185.5	8.02%	1642.7	821.4	3.56	**0.043**
Axis	1	15118.6	38.07%	10683.4	10683.4	46.28	**0.000**
2-Way Interactions	6	4376.0	11.02%	4376.0	729.3	3.16	**0.018**
Voltage (V)*Speed (µm/s)	4	4094.3	10.31%	3530.2	882.6	3.82	**0.014**
Voltage (V)*Axis	2	281.7	0.71%	281.7	140.8	0.61	0.551
Error	27	6233.0	15.70%	6233.0	230.9		
Lack-of-Fit	2	1180.5	2.97%	1180.5	590.2	2.92	0.072
Pure Error	25	5052.5	12.72%	5052.5	202.1		
Total	38	39709.4	100.00%				

Then, the speed had a significant effect on width, as shown in the interaction plot in Fig. 18a; it illustrates the same trends previously shown while the interaction plots have shown the same pattern with the low voltage and high speed, while a slight interaction happened between 0.25 µm/s and 0.5 µm/s, and similarly with the axis of two having the highest averages across speed and voltage. The speed was not used in the interaction model since it was missing the intermediate level introduced in Y-vibration.

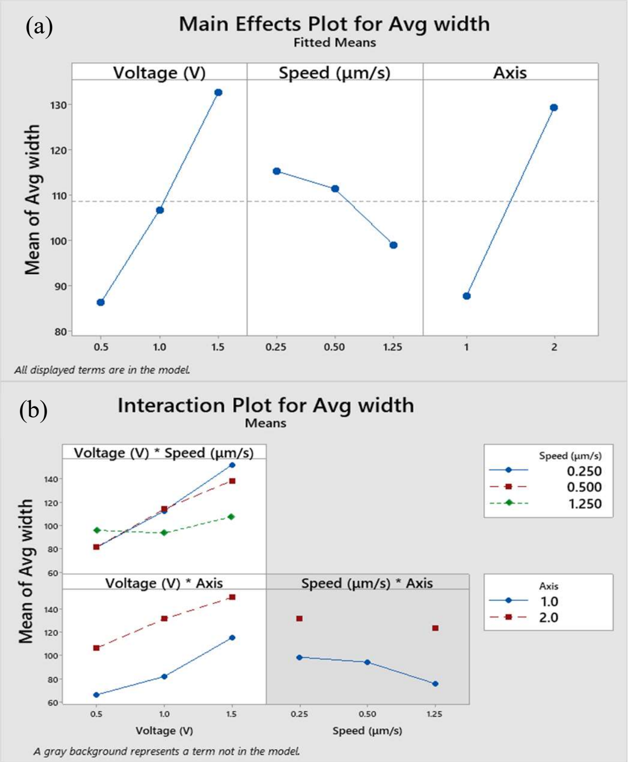

Fig. 18. (a) Main effect plot of average width in combined DOE dataset. (b) Interaction plot of average width in combined DOE dataset.

Predictions from the combined DOE datasets of the depth and width of the trenches are illustrated in Fig. 19a and Fig. 19b respectively.

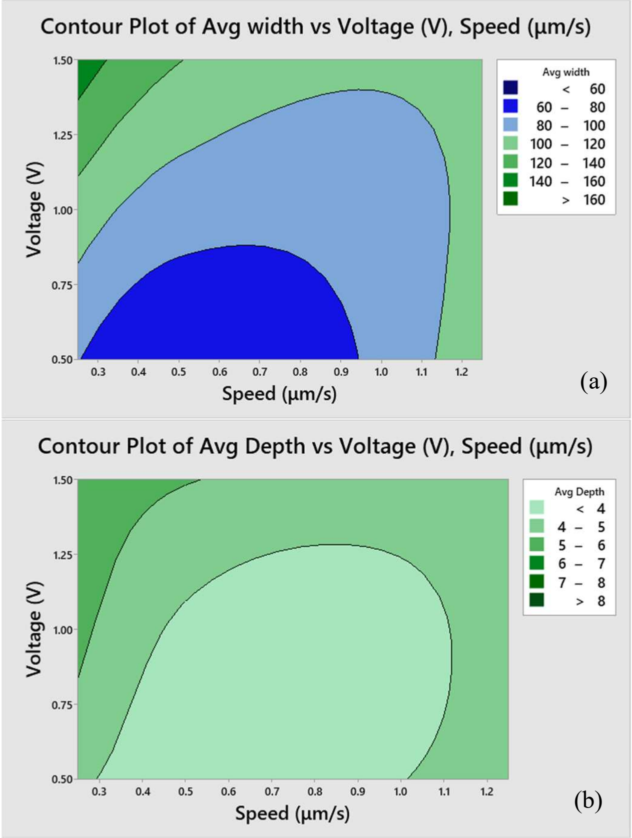

Fig. 19. (a) Contour plot of the depth versus the voltage and speed. (b) Contour plot of the width versus the voltage and speed.

In our previous study [36], we conducted experiments on PMMA film to examine vibration and electrical field-assisted nanolithography parameters. We used a similar setup and probe with the same spring constant as in this work but with variations in the design of the vibration stage. Table 11 presents a comparison of the results between our previous studies and the current work. Similar depth values are observed across a range of low to intermediate speeds and various vibration amplitudes. However, notable differences in width values could be attributed to variations in setpoint values, sample stage setup, and the conductivity of the thin film.

Table 11. Comparison of experiments of XY-vibration-assisted E-AFM at different parameters.

Film material	Voltage (V)	Vibration amplitude (Vpp)	Setpoint (nN)	Speed (µm)	Average Depth (nm)	Average Width (nm)
PEDOT	0.5	0.2	2	0.25	4.5	101
	1				6.2	134
	1.5				7.1	159
PMMA	0.5	0.6	0.1	0.5	4.2	38
	1				5.8	56
	1.2				7	68

5. Conclusion

In conclusion, this study demonstrated the possibility of nanopatterning on PEDOT: PSS using an electric field and vibration-assisted AFM-based nanopatterning method. We systematically investigated the effects of various experimental parameters on the nanolithography process. The results showed that using circular trajectory XY-vibration, optimized speed, and voltage factors could significantly improve the resolution and quality of the lithography patterns based on the resolution of patterns needed regarding width and depth. On the other hand, for lower depth and width applications, the Y-vibration with a reciprocating motion could be considered for better trench width. The Pareto chart analysis also revealed the relative importance of each parameter in the process. The results revealed that voltage, speed, and number of axes of vibration significantly influenced the width and depth of the lithography patterns.

Under XY-vibration, voltage primarily controls the pattern width, while speed has a more significant effect on pattern depth. In contrast, under Y-vibration, voltage plays the most significant role in both width and depth control. The study also finds that there is a minimum threshold of speed required to produce patterns, and the choice of vibration trajectory affects the achievable resolution and pattern formation due not only to the dynamic force introduced by the vibration but also to the distribution of the electrical field along the trajectory as well. Overall, this investigation provides valuable insights into the optimization of AFM-based nanofabrication techniques, particularly for applications in organic electronics and nanoelectromechanical systems. The findings can guide the development of high-resolution nanomanufacturing processes and contribute to the advancement of nanotechnology-enabled devices and systems.

Acknowledgments

This work was partly supported by the National Science Foundation under Grant No. CMMI-2006127, by a Binghamton University Data Science Transdisciplinary Area of Excellence (TAE) seed grant, and by the Small Scale Systems Integration and Packaging (S3IP) Centre of Excellence, funded by New York Empire State Development's Division of Science, Technology and Innovation.

References

[1] Y. Huang, X. Duan, Q. Wei, and C. M. Lieber, “Directed assembly of one-dimensional nanostructures into functional networks,” *Science*, vol. 291, no. 5504, pp. 630–633, Jan. 2001, doi: 10.1126/SCIENCE.291.5504.630.

[2] I. W. Rangelow *et al.*, “Nanoprobe maskless lithography,” *Alternative Lithographic Technologies II*, vol. 7637, p. 76370V, Mar. 2010, doi: 10.1117/12.852265.

[3] M. Cai *et al.*, “Extremely Efficient Indium–Tin-Oxide-Free Green Phosphorescent Organic Light-Emitting Diodes,” *Advanced Materials*, vol. 24, no. 31, pp. 4337–4342, Aug. 2012, doi: 10.1002/ADMA.201202035.

[4] K. Hong *et al.*, “Photopatternable, highly conductive and low work function polymer electrodes for high-performance n-type bottom contact organic transistors,” *Org Electron*, vol. 12, no. 3, pp. 516–519, Mar. 2011, doi: 10.1016/J.ORGEL.2010.12.022.

[5] P. Andersson Ersman, D. Nilsson, J. Kawahara, G. Gustafsson, and M. Berggren, “Fast-switching all-printed organic electrochemical transistors,” *Org Electron*, vol. 14, no. 5, pp. 1276–1280, May 2013, doi: 10.1016/J.ORGEL.2013.02.027.

[6] S. I. Na, S. S. Kim, J. Jo, and D. Y. Kim, “Efficient and Flexible ITO-Free Organic Solar Cells Using Highly Conductive Polymer Anodes,” *Advanced Materials*, vol. 20, no. 21, pp. 4061–4067, Nov. 2008, doi: 10.1002/ADMA.200800338.

[7] M. C. Barr, C. Carbonera, R. Po, V. Bulović, and K. K. Gleason, “Cathode buffer layers based on vacuum and solution deposited poly(3,4-ethylenedioxythiophene) for efficient inverted organic solar cells,” *Appl Phys Lett*, vol. 100, no. 18, p. 183301, Apr. 2012, doi: 10.1063/1.4709481/528718.

[8] D. Khodagholy *et al.*, “Highly Conformable Conducting Polymer Electrodes for In Vivo Recordings,” *Advanced Materials*, vol. 23, no. 36, pp. H268–H272, Sep. 2011, doi: 10.1002/ADMA.201102378.

[9] D. Khodagholy *et al.*, “In vivo recordings of brain activity using organic transistors,” *Nature Communications 2013 4:1*, vol. 4, no. 1, pp. 1–7, Mar. 2013, doi: 10.1038/ncomms2573.

[10] O. Y. Posudievsky, N. V. Konoshchuk, A. G. Shkavro, V. G. Koshechko, and V. D. Pokhodenko, “Structure and electronic properties of poly(3,4-ethylenedioxythiophene) poly(styrene sulfonate) prepared under ultrasonic irradiation,” *Synth Met*, vol. 195, pp. 335–339, Sep. 2014, doi: 10.1016/J.SYNTHMET.2014.07.001.

[11] G. Venugopal and S.-J. Kim, “Nanolithography,” *Advances in Micro/Nano Electromechanical Systems and Fabrication Technologies*, May 2013, doi: 10.5772/55527.

[12] E. M. Sebastian, S. K. Jain, R. Purohit, S. K. Dhakad, and R. S. Rana, “Nanolithography and its current advancements,” *Mater Today Proc*, vol. 26, pp. 2351–2356, Jan. 2020, doi: 10.1016/J.MATPR.2020.02.505.

[13] G. Venugopal, S.-J. Kim, G. Venugopal, and S.-J. Kim, “Nanolithography,” *Advances in Micro/Nano Electromechanical Systems and Fabrication Technologies*, May 2013, doi: 10.5772/55527.

[14] D. Resnick, “Nanoimprint lithography,” *Nanolithography: The Art of Fabricating Nanoelectronic and Nanophotonic Devices and Systems*, pp. 315–347, 2013, doi: 10.1533/9780857098757.315.

[15] A. A. Tseng, A. Notargiacomo, and T. P. Chen, “Nanofabrication by scanning probe microscope lithography: A review,” *Journal of Vacuum Science & Technology B: Microelectronics and Nanometer Structures Processing, Measurement, and Phenomena*, vol. 23, no. 3, pp. 877–894, May 2005, doi: 10.1116/1.1926293.

[16] L. G. Rosa and J. Liang, “Atomic force microscope nanolithography: dip-pen, nanoshaving, nanografting, tapping mode, electrochemical and thermal nanolithography,” *Journal of Physics: Condensed Matter*, vol. 21, no. 48, p. 483001, Nov. 2009, doi: 10.1088/0953-8984/21/48/483001.

[17] R. P. Seisyan, “Extreme ultraviolet nanolithography for ULSI: A review,” *Technical Physics*, vol. 50, no. 5, pp. 535–545, 2005, doi: 10.1134/1.1927207/METRICS.

[18] H. I. Smith and M. L. Schattenburg, “X-ray lithography, from 500 to 30 nm: X-ray nanolithography,” *IBM J Res Dev*, vol. 37, no. 3, pp. 319–329, 1993, doi: 10.1147/RD.373.0319.

[19] M. Kaestner *et al.*, “Scanning probes in nanostructure fabrication,” *Journal of Vacuum Science & Technology B, Nanotechnology and Microelectronics: Materials, Processing, Measurement, and Phenomena*, vol. 32, no. 6, Nov. 2014, doi: 10.1116/1.4897500/103332.

[20] J. Zhang, T. Cui, C. Ge, Y. Sui, and H. Yang, “Review of micro/nano machining by utilizing elliptical vibration cutting,” *Int J Mach Tools Manuf*, vol. 106, pp. 109–126, Jul. 2016, doi: 10.1016/J.IJMACHTOOLS.2016.04.008.

[21] Y. Yan, S. Chang, T. Wang, and Y. Geng, “Scratch on Polymer Materials Using AFM Tip-Based Approach: A Review,” *Polymers (Basel)*, vol. 11, no. 10, Oct. 2019, doi: 10.3390/POLYM11101590.

[22] J. Deng, J. Dong, and P. H. Cohen, “Development and Characterization of Ultrasonic Vibration Assisted Nanomachining Process for Three-Dimensional Nanofabrication,” *IEEE Trans Nanotechnol*, vol. 17, no. 3, pp. 559–566, May 2018, doi: 10.1109/TNANO.2018.2826841.

[23] L. Zhang, J. Dong, and P. H. Cohen, “Material-insensitive feature depth control and machining force reduction by ultrasonic vibration in AFM-based nanomachining,” *IEEE Trans Nanotechnol*, vol. 12, no. 5, pp. 743–750, 2013, doi: 10.1109/TNANO.2013.2273272.

[24] X. Hou *et al.*, “High-rate tunable ultrasonic force regulated nanomachining lithography with an atomic force microscope,” *Nanotechnology*, vol. 23, no. 8, p. 085303, Feb. 2012, doi: 10.1088/0957-4484/23/8/085303.

[25] J. Shi, L. Liu, P. Zhou, F. Wang, and Y. Wang, “Subnanomachining by ultrasonic-vibration-assisted atomic force microscopy,” *IEEE Trans Nanotechnol*, vol. 14, no. 4, pp. 735–741, Jul. 2015, doi: 10.1109/TNANO.2015.2439311.

[26] J. Deng, L. Zhang, J. Dong, and P. H. Cohen, “AFM-based 3D Nanofabrication Using Ultrasonic Vibration Assisted Nanomachining,” *Procedia Manuf*, vol. 1, pp. 584–592, Jan. 2015, doi: 10.1016/J.PROMFG.2015.09.036.

[27] D. E. Brehl and T. A. Dow, “Review of vibration-assisted machining,” *Precis Eng*, vol. 32, no. 3, pp. 153–172, Jul. 2008, doi: 10.1016/J.PRECISIONENG.2007.08.003.

[28] J. Deng, L. Jiang, B. Si, H. Zhou, J. Dong, and P. Cohen, “AFM-Based nanofabrication and quality

inspection of three-dimensional nanotemplates for soft lithography," *J Manuf Process*, vol. 66, pp. 565–573, Jun. 2021, doi: 10.1016/J.JMAPRO.2021.04.051.

[29] H. Zhou, C. Dmuchowski, C. Ke, and J. Deng, "External-energy-assisted nanomachining with low-stiffness atomic force microscopy probes," *Manuf Lett*, vol. 23, pp. 1–4, Jan. 2020, doi: 10.1016/J.MFGLET.2019.11.001.

[30] L. Li, M. Hirtz, W. Wang, C. Du, H. Fuchs, and L. Chi, "Patterning of Polymer Electrodes by Nanoscratching," *Advanced Materials*, vol. 22, no. 12, pp. 1374–1378, Mar. 2010, doi: 10.1002/ADMA.200902941.

[31] S. F. Lyuksyutov *et al.*, "Electrostatic nanolithography in polymers using atomic force microscopy," *Nature Materials 2003 2:7*, vol. 2, no. 7, pp. 468–472, Jun. 2003, doi: 10.1038/nmat926.

[32] J. N. Randall *et al.*, "Highly parallel scanning tunneling microscope based hydrogen depassivation lithography," *Journal of Vacuum Science & Technology B, Nanotechnology and Microelectronics: Materials, Processing, Measurement, and Phenomena*, vol. 36, no. 6, pp. 6–11, Nov. 2018, doi: 10.1116/1.5047939/16714023/06JL05_1_ACCEPTED_MANUSCRIPT.PDF.

[33] J. A. Dagata, "SPM-based lithography for electronics device fabrication: new strategies and directions," *Materials Research Society Symposium - Proceedings*, vol. 380, no. 1, pp. 153–162, Feb. 1995, doi: 10.1557/PROC-380-153/METRICS.

[34] J. A. Dagata, "Device Fabrication by Scanned Probe Oxidation," *Science (1979)*, vol. 270, no. 5242, pp. 1625–1626, Dec. 1995, doi: 10.1126/SCIENCE.270.5242.1625.

[35] H. Zhou, Y. Jiang, C. M. Dmuchowski, C. Ke, and J. Deng, "Electric-Field-Assisted Contact Mode Atomic Force Microscope-Based Nanolithography With Low Stiffness Conductive Probes," *J Micro Nanomanuf*, vol. 10, no. 1, Mar. 2022, doi: 10.1115/1.4054316/1140106.

[36] H. Zhou, Y. Jiang, C. Ke, and J. Deng, "Electric-Field and Mechanical Vibration-Assisted Atomic Force Microscope-Based Nanopatterning," *J Micro Nanomanuf*, vol. 10, no. 2, Jun. 2022, doi: 10.1115/1.4056731.